Modeling of plasma and plasma-surface interactions for medical, environmental and nano applications

2012 J. Phys.: Conf. Ser. 399 012011

(http://iopscience.iop.org/1742-6596/399/1/012011)

Journal of Physics: Conference Series **399** (2012) 012011 doi:10.1088/1742-6596/399/1/012011

Modeling of plasma and plasma-surface interactions for medical, environmental and nano applications

A Bogaerts, R Aerts, R Snoeckx, W Somers, W Van Gaens, M Yusupov and E Neyts

Research group PLASMANT, University of Antwerp, Dept of Chemistry, Universiteitsplein 1, B-2610 Wilrijk, Belgium

Annemie.bogaerts@ua.ac.be

Abstract. In this paper, an overview is given of modeling investigations carried out in our research group for a better understanding of plasmas used for medical, environmental and nano applications. The focus is both on modeling the plasma chemistry and the plasma-surface interactions. The plasma chemistry provides the densities and fluxes of the important plasma species. This information can be used as input when modeling the plasma-surface interactions. The combination of plasma simulations and plasma – surface interaction simulations provides a more comprehensive understanding of the underlying processes for these applications.

1. Introduction

Gas discharge plasmas are used for a large number of applications. In recent years, there is a growing interest for medical, environmental and nano applications. Plasma medical applications include sterilization of, among others, heat-sensitive (surgery) equipment, deposition of biocompatible coatings, as well as therapeutic applications, such as wound healing, dental treatment, cancer treatment, microsurgery,… Details can be found in the many review papers and in several books (e.g., [1-3]). Environmental applications comprise air and water purification, volatile organic compound decomposition, as well as the conversion of greenhouse gases into value-added chemicals (e.g., [4-6]). Finally, nano applications include the fabrication of nanoscale devices by etching and deposition steps, as well as the growth of nanostructured materials, such as carbon nanotubes, graphene, nanowires,…(e.g., [7-9]).

To improve these applications, a good insight in the underlying physical and chemical processes, occurring in the plasma itself and in interaction with a substrate, is desirable. This can be obtained by experiments, but measurements inside the plasma are not always straightforward because of the small plasma dimensions. Moreover, detailed information, such as species densities, can only be achieved by dedicated and expensive (laser) diagnostics. An alternative is to obtain this information by computer modeling, i.e., by describing the behavior of the various plasma species inside the plasma, as well as their interactions with the surface. This is the focus of the present paper.

There exist different modeling approaches in literature for describing plasmas, such as analytical models (e.g., [10]), solving the Boltzmann equation (e.g., [11]), zero-dimensional (0D) chemical kinetics models (e.g., [12]), 1D or 2D fluid models (e.g., [13]), Monte Carlo (MC) and particle-in-cell – Monte Carlo collision (PIC-MCC) simulations (e.g., [14-15]), as well as hybrid models (e.g., [16]), which are a combination of the above models. Each of these models has its specific advantages and disadvantages. For describing a detailed plasma chemistry, which is the focus of our work, 0D

chemical kinetics models or fluid models are the most convenient, as they can describe a large number of different plasma species without too much computational effort. Also hybrid MC-fluid models can be applied, when the plasma chemistry is treated in the fluid part. The examples that will be presented in this paper are obtained with either 0D chemical kinetics models or with a 2D hybrid model.

Modeling the plasma-surface interactions can be performed with detailed atomistic molecular dynamics (MD) simulations (e.g., [17-18]) or with MC or analytical surface kinetics models (e.g., [19]). However, in the latter case, the surface reaction coefficients are needed as input in the model. This is not required in MD simulations, which describe the behavior of all the atoms in the system in a self-consistent, deterministic way, without the need of *a priori* knowledge on the reaction mechanisms. The major disadvantage of MD simulations is the long calculation time, limiting both the attainable time and length scales. Moreover, an accurate interatomic interaction potential must be available for realistic simulations..

In the following sections, we will present some examples of modeling work for the plasma chemistry and plasma-surface interactions, carried out in our research group, for medical, environmental and nano applications, to illustrate the kind of information that can be obtained with this kind of modeling.

2. Medical applications

2.1. Modeling the plasma chemistry

A range of different plasma source designs have been developed for plasma medical applications, but the plasma jet type is quite often used. In our work, we consider a plasma jet formed by a needle electrode, as designed by Hofman and Bruggeman [20] and by Leys and coworkers [21]. In order to obtain a better understanding of the important plasma species in this plasma jet, we have developed a detailed plasma chemistry set for an Ar plasma, flowing into ambient (humid) air (i.e., N_2, O_2 and H_2O). The species taken into account in this model are listed in Table 1.

Table 1. Overview of the species included in the model for the Ar plasma jet flowing into ambient humid air.

Ground state species	Excited species	Charged species
Ar	$Ar(^4S)$, $Ar(^4P)$, Ar_2^* ($a\ ^3\Sigma^+_u$)	e^-, Ar^+, Ar_2^+
N_2, N	$N_{2\ vibrational}$, $N_{2\ rotational}$, $N_2(A\ ^3\Sigma^+_u)$, N_2 ($a'\ ^1\Sigma^-_u$), $N(^2D)$,	N_2^+, N_3^+, N_4^+, N^+
O_2, O_3, O	$O_{2\ vibrational}$, $O_{2\ rotational}$, O_2 ($a\ ^1\Delta_g$), O_2 ($b\ ^1\Sigma^+_g$), $O(^1D)$	O_2^+, O_4^+, O^+, O^-, O_2^-, O_3^-
NO, NO_2, N_2O, NO_3, N_2O_3, N_2O_4, N_2O_5		NO^+, NO_2^+, NO_2^-, NO_3^-
H_2, H, NH, HNO, HNO_2, HNO_3, HNO_4	$H_{2\ vibrational}$, $H_{2\ rotational}$	H^+, H_2^+, H_3^+, H^-, ArH^+
H_2O, H_2O_2, HO_2 , OH	$H_2O_{\ vibrational}$	H_2O^+, H_3O^+, $H_2O_2^-$, OH^+, OH^-

These species react with each other in a large number of collisions. In total, 264 electron impact collisions, 796 ion reactions and 591 neutral reactions are taken into account. More detailed information about this reaction set, as well as the corresponding rate coefficients or cross sections, can be found in [22].

The density evolution of these species, based on the production and loss processes as defined by these chemical reactions, is calculated by means of a 0D chemical kinetics model, developed by Kushner and coworkers, called Global_kin [12]. The rate coefficients of the ion and neutral reactions are assumed constant, dependent only on the gas temperature. The rate coefficients of the electron impact reactions are a function of the electron energy. They are calculated by a Boltzmann solver for a wide range of reduced electric field values, and subsequently tabulated as a function of electron energy. The electron energy is calculated with an energy balance equation, based on energy gain due to Joule heating and energy loss due to elastic and inelastic collisions.

Although Global_kin is a 0D model, it is used in our work to calculate the densities of the various plasma species as a function of position from the needle, as well as in the flowing afterglow of the plasma jet, by converting the spatial variation into a time variation, based on the flow velocity. Hence, the species densities in a certain volume element are calculated as a function of time, treating this volume element as a batch reactor, but mimicking the condition of a cylindrical plug flow reactor, where this volume element moves in one direction, along the needle axis and beyond, as if the species densities vary as a function of distance. For this purpose, a certain power profile is applied, with a maximum at the needle tip, and decreasing towards the flowing afterglow (see Figure 1 below). Moreover, the mixing of the flowing Ar plasma jet with the ambient air is described by assuming certain concentration profiles of the background gases, mimicking the diffusion process of the humid air gases into the argon flow. This means that the Ar gas density corresponds to atmospheric pressure inside the needle device, but drops to lower values in the ambient air region, and the opposite is true for N_2, O_2 and H_2O. The background gas densities, as well as the calculated electron density and electron temperature, are plotted as a function of position from the needle tip, both inside the plasma jet device and in the afterglow, in Figure 1.

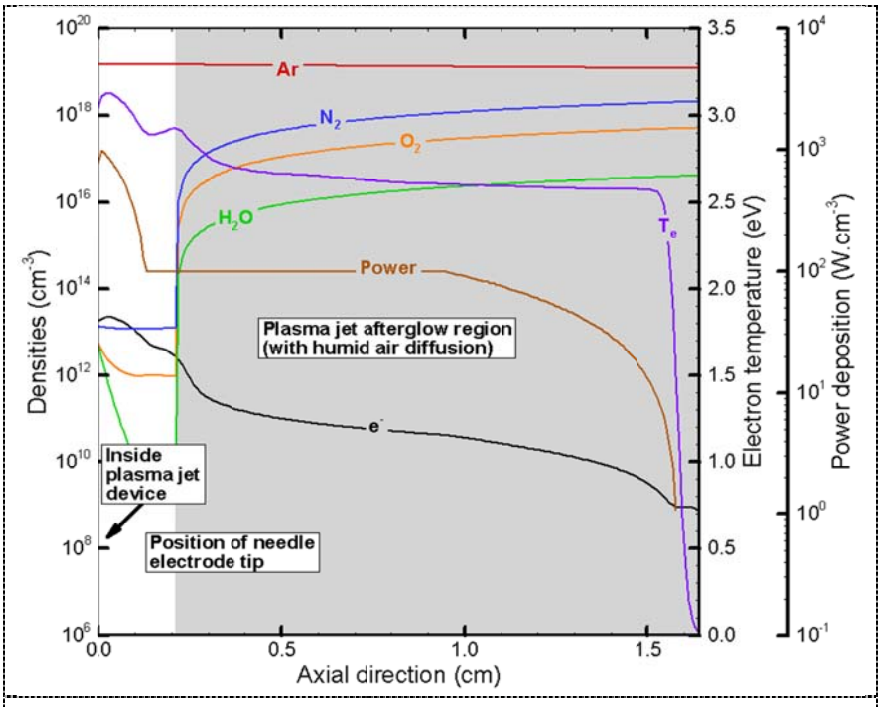

Figure 1. Densities of the background gases, as well as electron density and temperature, as a function of position from the needle tip, inside the plasma jet device and in the afterglow region.

The calculated densities of biomedically important species in the plasma jet afterglow region are illustrated in Figure 2. It is clear that O, O_3, NO, N, H, OH and H_2O_2 are present in large amounts. The O density, however, drops after about 1 cm from the needle tip, whereas the O_3 density, which is negligible near the needle tip, rises as a function of distance and becomes even higher than the O density. Furthermore, OH will convert into H_2O_2 after roughly 1.2 cm. Our calculations also predict that cluster formation is important in the ion chemistry. More details can be found in a forthcoming paper [22].

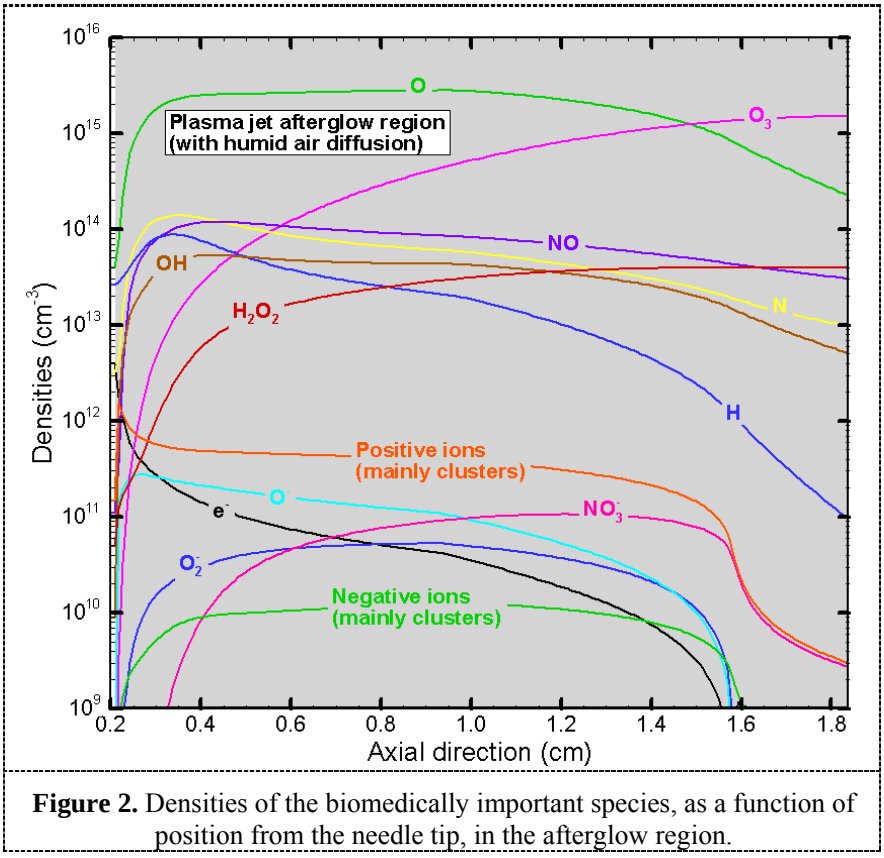

Figure 2. Densities of the biomedically important species, as a function of position from the needle tip, in the afterglow region.

2.2. Modeling the plasma-cell interactions

To elucidate the effect of plasma species for biomedical applications, it is of interest to study their detailed behavior when interacting with living cells. We use MD simulations for this purpose, and in a first attempt, we consider the interaction of plasma species with a bacterial cell wall, for sterilization purposes. More specifically, we describe the interaction with peptidoglycan (PG), which is the outer layer of the cell wall of gram-positive bacteria, such as Staphylococcus aureus.

The PG structure is already quite complicated, and consists of disaccharide layers, stem (tetrapeptide) and bridge (pentaglycine), as is shown schematically in Figure 3. More details about this structure can be found in [23].

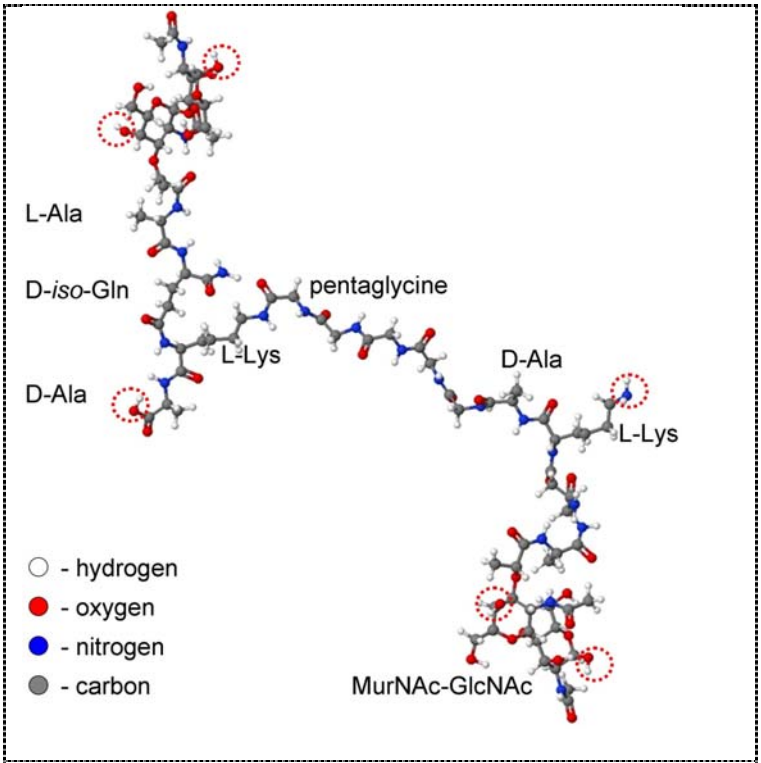

Figure 3. Structural unit of PG, as used for the MD simulations

The interaction of plasma species with this PG is described by atomic scale MD simulations. The behavior of all the atoms in the system, i.e., originating from the impacting plasma species, as well as from the PG structure, is followed as a function of time by solving Newton's laws. The forces acting on all the atoms are derived from the interatomic interaction potential. In our work, we assume the Reax force field (ReaxFF), developed by van Duin and coworkers [24], and the parameters describing the C-N-O-H interactions are adopted from [25].

The plasma species considered in this study, include O, OH, O_3 and O_2. They were found to be important in the plasma jet, as shown in Figure 2 above, but it is no guarantee that they are also the important species interacting with the bacterial cell walls. Indeed, the bacteria are typically covered by a liquid layer (biofilm) and it is well possible that the important plasma species react in this layer, with the formation of other species. This process will be investigated in our future work. However, as a first step, we consider here the interaction of O, OH, O_3 and O_2 species, to obtain some first insight in the possible role that plasma species can play when interacting with bacterial cell walls.

Our calculations predict that O_2 molecules do not result in bond breaking of the PG structure, but the other species investigated, i.e., O, OH and O_3, do result in the breaking of some important C-C, C-N and C-O bonds, and this can give rise to bacterial cell wall damage. We found that the C-O bonds in the disaccharide molecules are most easily broken, followed by the C-C bonds and the C-N bonds. The O atoms appear to be the most reactive, as is clear from Table 2. This table shows the fraction of C-N, C-O and C-C bond breaking events, upon impact of O, O_3 and OH species, when following the species for a sufficiently long time. As mentioned above, it is well possible that other plasma species will interact with the bacterial cell wall, instead of the species studied here. But this example is only the first step in our investigations, and it illustrates that MD simulations can be very valuable for obtaining atomic scale insight in the underlying mechanisms of plasma medicine. More detailed information, including insight in the bond breaking mechanisms, can be found in [23].

Table 2. Summary of the fraction of C-N, C-O and C-C bonds (in %) that break in the PG structure upon impact of O, O_3 and OH species, as obtained from MD simulations.

Incident plasma species	C-N bonds	C-O bonds	C-C bonds
O atoms	26	78	38
OH radicals	8	54	14
O_3 molecules	8	56	26

3. Environmental applications

3.1. Modeling the plasma chemistry

As mentioned in the introduction, plasmas are used for various environmental applications. The application we are most interested in, is the conversion of greenhouse gases (CO_2, CH_4) into value-added chemicals or new fuels. We performed simulations for a dielectric barrier discharge (DBD) reactor, consisting of two concentric cylinders, with a gap of a few mm, through which the gas is flowing. Again the 0D chemical kinetics code Global_kin [12] was applied. The advantage of this code is that the occurrence of filaments in the DBD plasma can be approximated, by considering a large number of power pulses as a function of time. This is explained in more detail in [26,27].

We investigated the splitting of CO_2 [26], as well as the dry reforming reaction between CO_2 and CH_4 [27]. The species taken into account in the CO_2 plasma are listed in Table 3. They include not only ground state species, but also a large number of vibrationally and electronically excited species, as is clear from this Table. These species react in 240 electron impact collisions, 176 ion and 85 neutral reactions. More details about this plasma chemistry set can be found in [26].

Table 3. Overview of the species included in the model for the CO_2 splitting.

Ground state species	Excited species	Charged species
CO_2, CO, C_2O	CO_2 v1 (010)	CO_2^+, CO_4^+, CO^+
C, C_2	CO_2 v2 ((100), (020))	$C_2O_2^+$, $C_2O_3^+$,
O_2, O_3, O	CO_2 v3 (001)	$C_2O_4^+$
	CO_2 v4 ((n00), (0n0))	
	$CO_2(^1\Pi_g)$	C^+, C_2^+, CO_3^-,
	$CO_2(^1\Delta_u)$	CO_4^-
	COv1 (sum of vibrations)	
	$CO(A^3\Pi)$	O_2^+, O^+, O_4^+
	$CO(A^1\Pi)$	
	Sum of ($CO(A^3\Sigma)$, $CO(D^3\Delta)$, $CO(E^3\Sigma)$, $O(B^3\Sigma)$)	O^-, O_2^-, O_3^-, O_4^-
	Sum of ($CO(C^1\Sigma)$, $CO(E^1\Pi)$, $CO(B^1\Sigma)$, $CO(I^1\Sigma)$, $CO(D^1\Delta)$	Electrons
	O_2 v1 (n_v=1,2)	

It is stated by Fridman that the vibrationally excited CO_2 molecules can play a significant role in the plasma, and in the CO_2 splitting process, depending on the type of plasma [28]. Indeed, when the reduced electric field is in the order of 1-100 Td, and the electron temperature is around 1 eV, up to 97% of the energy can go into the vibrationally excited levels [28]. However, in the DBD discharge under study, the reduced electric field is typically above 200 Td, so it is expected that the vibrationally excited levels play a more moderate role. This was investigated in detail in [26]. Figure 4 shows the ground state density of CO_2, as well as the densities of the four vibrationally excited states, taken into account in the model, during one discharge pulse and its afterglow (a), as well as for five consecutive pulses with an interpulse time of 1 μs (b). It is clear from Figure 4(a) that the ground state density slightly drops when the discharge pulse starts, and the vibrationally excited states are formed. Upon pulse termination, the higher vibrationally excited levels will decay to the lower levels by V-V transitions, and this leads to a further increase of the lowest excited level (CO_2v1). However, after about 10 μs, this lowest excited level will also fall back to the ground state by V-T transitions, so that the ground state density rises again to more or less its initial value before the pulse. When five consecutive discharge pulses are followed (see Figure 4(b)), some accumulation effect can be observed, especially for the lower vibrationally excited densities, and after these five pulses, the density of the lowest vibrational level is only a factor of three lower than the ground state density.

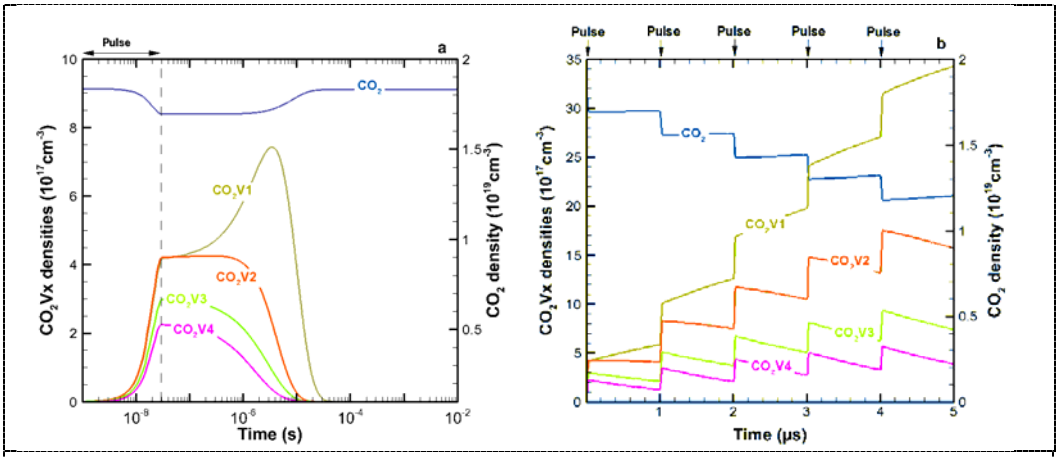

Figure 4. Calculated densities of the CO_2 ground state and four different vibrationally excited levels, in a DBD reactor, for one discharge pulse (filament) and its afterglow (a), as well as for five consecutive discharge pulses (filaments) with an interpulse time of 1 μs (b).

It should be noted that the consecutive pulses are applied in the model, to mimic the filamentary behavior of a DBD. This is a very approximative way, as we do not describe the filament formation process itself, but nevertheless it can give us some insight in the filamentary character of the DBD and its effect on gas conversion. We expect that the CO_2 gas molecules will pass several filaments when they flow through the DBD reactor, but the exact number of filaments they pass, and the typical time in between such filaments is actually not known. We have therefore investigated the effect of the interpulse time on the formation of the vibrationally excited levels, as well as on the fall back ratio of these levels, and the result is illustrated in Figure 5. It is clear from Figure 5(a) that for an interpulse time below 1 μs, a strong accumulation of the vibrationally excited levels is observed, as was also clear from Figure 4(b) above, and the fall back is found to be negligible (see Figure 5(b)). However, at an interpulse time above 10 μs, the accumulation effect is found to be negligible, and nearly all vibrationally excited levels will relax back the ground state. Therefore, the importance of the vibrationally excited levels will strongly depend on the actual interpulse time, or time between two filaments which the CO_2 molecules pass, in the DBD reactor.

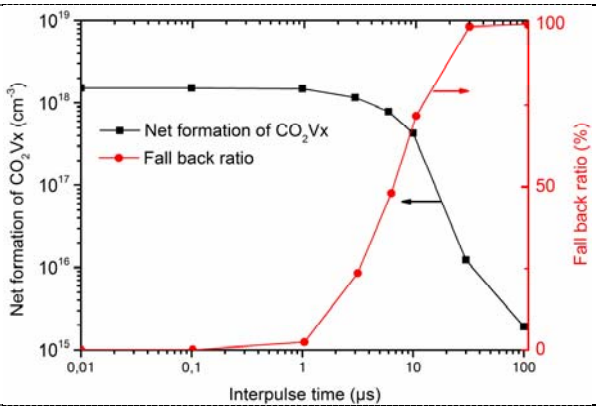

Figure 5. Calculated net formation of vibrationally excited CO_2 molecules (black curve; left axis), and fall back ratio to the ground state (red curve; right axis), as a function of the interpulse time, for consecutive discharge pulses (filaments).

The species considered in the model for the dry reforming process, i.e., in the CH_4/CO_2 gas mixture, are listed in Table 4. As is clear, several higher hydrocarbon species are included in the model, as well as possible interesting end products, such as syngas (CO/H_2), methanol (CH_3OH) and formaldehyde (CH_2O). These species react in 121 electron impact collisions, 87 ion reactions and 290 neutral reactions.

Table 4. Overview of the species included in the model for CH_4/CO_2 dry reforming.

Ground state molecules	Excited species	Charged species	Radicals
CH_4	CH_4*	CH_5^+, CH_4^+, CH_3^+, CH_2^+, CH^+	CH_3, CH_2, CH, C
C_2H_6, C_2H_4, C_2H_2	C_2H_6*, C_2H_4*, C_2H_2*	$C_2H_6^+$, $C_2H_5^+$, $C_2H_4^+$, $C_2H_3^+$, $C_2H_2^+$	C_2H_5, C_2H_3, C_2H
C_3H_8, C_3H_6, C_4H_2	C_3H_8*		C_3H_7
H_2	H_2*		H
O_2	O*	O_2^+, O^-	O
CO_2, CO	CO_2*, CO*	CO_2^+	
H_2O, H_2O_2	H_2O*	H_3O^+, OH^-	OH, HO_2
CH_2O, CH_3OH,		Electrons	CHO, CH_2OH, CH_3O
CH_3CHO, CH_2CO			C_2HO, CH_3CO
			CH_2CHO, $C_2H_5O_2$

Similar results as illustrated above were also obtained for this gas mixture, i.e., we studied the detailed behavior of species densities during one microdischarge pulse and its afterglow, as well as for five consecutive pulses. Moreover, we also investigated the long time scale behavior of the dry reforming process, by considering a large number of consecutive discharge pulses, for a total time of

several seconds [27]. In this way, we could obtain information on the conversion of the CO_2 and CH_4 gas molecules, as well as on the selectivities of the reaction products, and on the energy cost and energy efficiency of the process, which is of course of primordial importance for this application. We cannot go into more detail here, due to space restrictions, but these results are presented in [27].

3.2. Modeling the plasma-catalyst interaction

Our plasma chemistry simulations reveal that the energy efficiency of the DBD reactor for greenhouse gas conversion is not yet competitive with existing classical reforming processes [27]. One way to improve the energy efficiency is by inserting a packing inside a DBD reactor, because this yields higher electric fields inside the voids between the packing pellets. Moreover, the pellets can be made of (or covered by) a catalytic material, which can improve the selectivity towards the desired end products. Currently, there is a lot of interest for so-called plasma catalysis, but again, the underlying mechanisms are not yet fully understood.

In an effort to obtain some better insight in the interaction mechanisms between plasma species and a catalyst surface, we performed MD simulations for the interaction of CH_3, CH_2 and CH species on a Ni surface, using again the ReaxFF force field, adopting parameters for the Ni-C-H system from [29]. Figure 6 illustrates, as an example, the molecules formed upon impact of CH_2 species on different Ni catalyst surfaces, i.e., Ni(111), which is the most stable Ni surface, and the most abundant surface facet in Ni catalysts [30], Ni(100), which has a higher surface energy and is also present in Ni catalysts [31], and two step-edged Ni(111) surfaces, since defect (step) sites may be formed at the catalyst surface [32]. It is clear that most CH_2 species are converted into CH_3 species, with a large fraction of non-adsorbed CH_3 species, and a minor fraction of adsorbed CH_3 species. Besides, also some CH_4, C_2H_4 and C_2H_6 molecules are formed, and even a small number of H_2 molecules, at least on the more reactive Ni(100) and stepped Ni(111) surfaces. More details can be found in [33]. These simulations are only a first step; in future work, we will investigate the effect of catalyst temperature and catalyst shape on the reactivity for different plasma species. Also other catalyst materials will be investigated in the future.

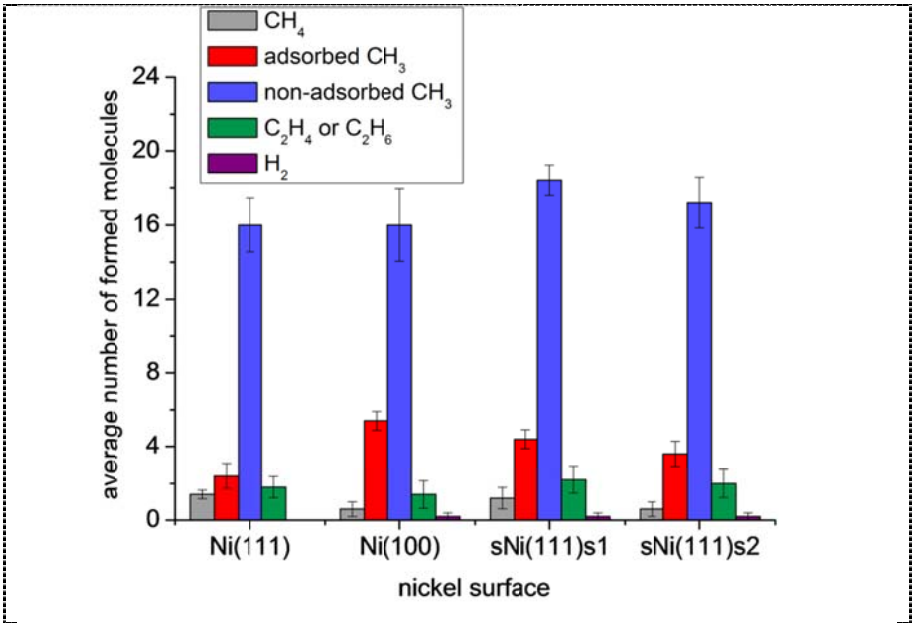

Figure 6. Molecules formed upon impact of CH_2 species on different Ni catalyst surfaces, as predicted by the MD simulations.

4. Nano applications

4.1. Modeling the plasma chemistry

CNT growth is one of the major topics under study in our group. CNTs are typically grown by catalytic chemical vapor deposition (CCVD), but we focus on plasma-based growth (PE-CVD). Most often, low pressure plasma's, such as inductively coupled plasma's (ICPs), are used for this purpose. At low pressure, a fluid (or 0D chemical kinetics) approach might be a too rough approximation, and therefore we made use of a hybrid MC – fluid model to describe the plasma chemistry. In the example shown here, we used the HPEM code, also developed by Kushner and coworkers [34].

CNTs can be grown in plasmas from different types of gas mixtures. Most commonly, a hydrocarbon gas (such as CH_4 or C_2H_2) is applied, in combination with a gas that can supply H-atoms (such as H_2 or NH_3) for etching the amorphous carbon from the CNT cap. We performed simulations for the different combinations, i.e., CH_4/H_2, C_2H_2/H_2, CH_4/NH_3 and C_2H_2/NH_3, to find out whether they yield a different plasma chemistry [35,36]. Again, a large number of different plasma species was taken into account, as is illustrated in Table 5 for the CH_4/NH_3 gas mixture. For more details about the chemistry sets, also for the other gas mixtures, we refer to [35].

Table 5. Overview of the species included in the model for the CH_4/NH_3 gas mixture.

Molecules	Radicals	Charged species
H_2	H	H^-, H_2^-, H_3^-
CH_4	C, CH, CH_2, CH_3	C^-, CH^-, CH_2^-, CH_3^-, CH_4^-, CH_5^-
C_2H_2, C_2H_4, C_2H_6	C_2, C_2H, C_2H_3, C_2H_5	C_2^-, C_2H^-, $C_2H_2^-$, $C_2H_3^-$, $C_2H_4^-$, $C_2H_5^-$,
C_3H_8, C_4H_{10}		$C_2H_6^-$
NH_3	NH_2, NH	NH^-, NH_2^-, NH_3^-, NH_4^-
N_2H_2, N_2H_4	N_2H, N_2H_3	
N_2, N_2*	N, N*	N^-, N_2^-
HCN	H_2CN, CN	HCN^-
		Electrons

Our calculations predicted that the major species formed in the plasma are H, H_2, CH_4, C_2H_2, C_2H_4, N, N_2, NH_3, HCN [35,36]. The C concentration appeared to be very low, indicating that the C supply for CNT growth should originate from decomposition of hydrocarbons at the catalyst surface itself.

4.2. Modeling the CNT growth

Finally, also the CNT growth itself is modeled with the MD approach. In fact, only the growth of single-walled carbon nanotubes (SWCNTs) is currently simulated with MD, and most often only the cap formation, because of the long calculation times. We modelled the SWCNT cap formation from a Ni catalyst particle, consisting of 40 atoms, and made again use of the ReaxFF potential, employing the parameters adopted from [29].

As mentioned above, the C supply for the CNT growth originates from decomposition of hydrocarbons at the catalyst surface. However, as this decomposition might take place on a longer time scale than is accessible by MD, we assumed that the Ni catalyst particle, either floating [37] or surface bound [38], is bombarded directly by C atoms. We extended our MD simulations with a MC method, in order to capture the surface reorganization in between two carbon impacts. This allowed us to obtain, for the first time, CNT caps with definable chiralities [37,38]. We were able to simulate the growth of both a semi-conducting SWCNT (with (12,4) chirality) [37], as well as a metallic SWCNT (with (7,7) chirality) [38]. Moreover, our simulations have demonstrated that the chirality can still change during the cap formation [38].

The above simulations hold true for SWCNT growth from CCVD. However, in [39] we made some attempts to describe the PE-CVD growth, by including the effect of an electric field. It was found that electric field values in the order of 300-700 kV/cm at the CNT tip yielded vertical alignment of the SWCNT cap, as seen in Figure 7. Lower electric field values result in a random nucleation point, whereas at higher electric field values no nucleation at all occurred. This range of electric field values seems high for typical plasmas, but near the CNT cap the local electric field can be much higher than in the sheath due to curvature effects. This field effect can be explained by the difference in electronegativity between C and Ni atoms, which implies that the C-Ni bonds are slightly polar, and can therefore be affected by the electric field. There will be a competition between diffusion and migration of the C atoms. At low electric field values, diffusion dominates and nucleation is random. At high electric field values, migration is more important, and hence oriented nucleation occurs [39].

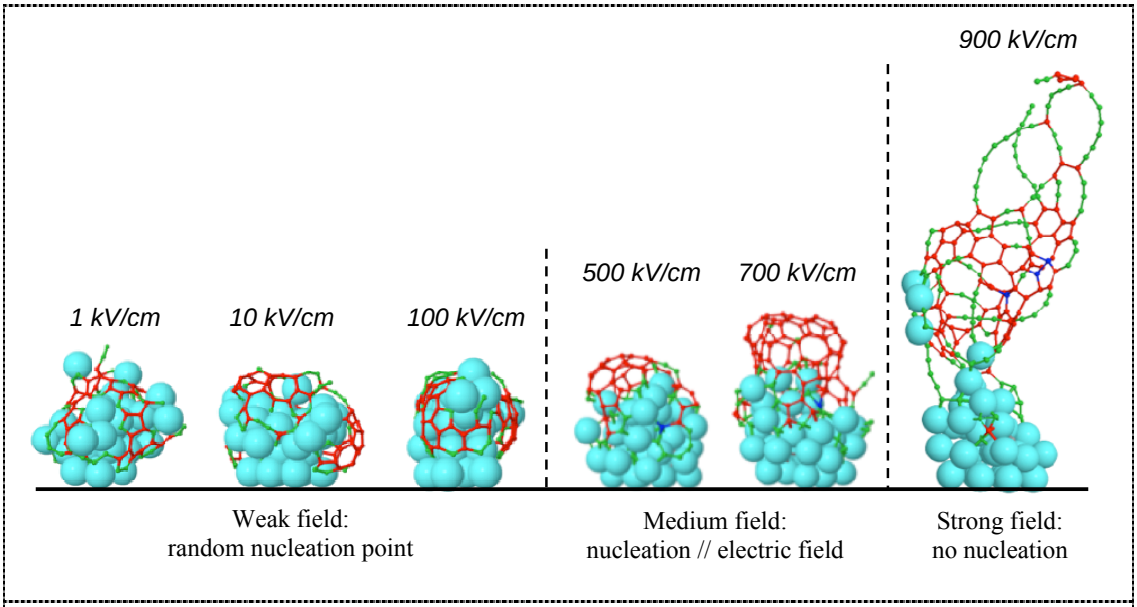

Figure 7. Effect of electric field on the nucleation of a SWNT. Reprinted with permission from [39], Copyright 2012 American Chemical Society

5. Conclusions

In this paper, we have shown some examples of modeling the plasma chemistry as well as plasma-surface interactions for plasma medicine, environmental and nano applications. For modeling the plasma chemistry, 0D chemical kinetics models or fluid models, or the fluid part of hybrid models are most suitable, as these model approaches can handle a large number of species without too much computational effort. These models give information on the densities and fluxes of the various species present in the plasma, as well as on the importance of the chemical reactions taking place in the plasma, yielding the production and loss of the various plasma species. Although a 0D model does not include spatial dimensions, it can still be used to give spatial information, as is illustrated here for a plasma jet (plasma needle). Moreover, a 0D model can approximate the filamentary behavior of a DBD reactor, by considering a large number of consecutive microdischarge pulses.

The plasma chemistry models provide information on the most important plasma species, which is of interest for plasma-surface interaction modeling. For this purpose we use MD simulations, which describe the behavior of the individual atoms in the system in a self-consistent way, without making approximations. We have shown examples in this paper from MD simulations for plasma medicine, i.e., the interaction of plasma species with bacterial cell walls, for plasma catalysis, i.e., the interaction of plasma species with Ni catalyst surfaces, and for nano applications, i.e., the growth of CNTs.

The plasma chemistry modeling and the atomic-scale MD simulations can give us a better insight in the plasma behavior and in its interaction with surfaces, respectively, which is of great importance for the applications.

References

[1] Dobrynin D, Fridman G, Friedman G, Fridman A 2009 *New J. Phys.,* **11** 115020
[2] Weltmann K D, von Woedtke T 2011 *IEEE Trans. Plasma Sci.* **39** 1015
[3] Laroussi M, Kong M G, Morfill G and Stolz W 2012 *Plasma Medicine: Applications of Low-Temperature Gas Plasmas in Medicine and Biology* (Cambridge University Press)
[4] Gutsol A, Rabinovich A, Fridman A 2011 *J. Phys. D: Appl. Phys.* **44** 274001
[5] Tu X, Gallon H J, Twigg M V, Gorry P A, Whitehead J C 2011 *J. Phys. D: Appl. Phys.* **44** 274007
[6] Fridman A, Chirokov A, Gutsol A 2005 *J. Phys. D: Appl. Phys.* **38** 1
[7] Vizireanu S, Stoica S D, Luculescu C, Nistor L C, Mitu B and Dinescu G 2010 Plasma Sources Sci. Technol. **19** 034016
[8] Ostrikov K, Cvelbar U and Murphy A B, 2011 *J. Phys. D: Appl. Phys.* **44** 174001
[9] Meyyappan M, 2011 *J. Phys. D: Appl. Phys.* **44** 174002
[10] Lee Y T, Lieberman M A, Lichtenberg A J, Bose F, Baltes H and Patrick R 1997 *J. Vac. Sci. Technol.* **15** 113
[11] Loffhagen D, Sigeneger F and Winkler R 2002 *J. Phys. D: Appl. Phys.* **35** 1768
[12] Dorai R, Kushner M and Hassouni K 2000 *J. Appl. Phys.* **88** 6060
[13] Passchier J D P, Goedheer W J 1993 *J. Appl. Phys.* **73** 1073
[14] Bogaerts A, van Straaten M and Gijbels R 1995 *Spectrochim. Acta Part B* **50** 179
[15] Bultinck E and Bogaerts A 2009 *New J. Phys.* **11** 103010
[16] Bogaerts A, Gijbels R and Goedheer W J 1995 *J. Appl. Phys.* **78** 2233
[17] Neyts E, Bogaerts A and van de Sanden M C M 2006 *J. Phys. D: Appl. Phys.* **39** 1948
[18] Graves D and Brault P 2009 *J. Phys. D: Appl. Phys.* **42** 194011
[19] Zhang D and Kushner M J 2000 *J. Appl. Phys.* **87** 1060
[20] Hofman S and Bruggeman P 2011 *IEEE Trans. Plasma Sci.* **39** 2332
[21] Li L, Nikiforov A, Xiong Q, Lu X, Taghizadeh L and Leys C 2012 *J. Phys. D: Appl. Phys.* **45** 125201
[22] Van Gaens W and Bogaerts A, paper in preparation
[23] Yusupov M, Neyts E C, Khalilov U, Snoeckx R, Van Duin A C T and Bogaerts A 2012 *New J. Phys.* (submitted).
[24] van Duin A C T, Dasgupta S, Lorant F and Goddard W A III 2001 *J. Phys. Chem. A* **105** 9396
[25] Rahaman O, van Duin A C T, Goddard W A III and Doren D J 2011 *J. Phys. Chem. B* **115** 249
[26] Aerts R, Martens T and Bogaerts A 2012 *J. Phys. Chem. C* (submitted).
[27] Snoeckx R, Aerts R and Bogaerts A, paper in preparation
[28] Fridman A 2008 *Plasma Chemistry* (New York: Cambridge University Press)
[29] Mueller J E, van Duin A C T, Goddard W A 2010 *J. Phys. Chem. C* **114** 4939
[30] Feng Q, Li T, Yue H, Qi K, Bai F and Jin J 2008 *Appl. Surf. Sci.* **254** 2262
[31] Huang Y Y, Shou Y C and Pan Y 2010 *Physica B* **405** 1335
[32] Bengaard H S, Norskov J K, Sehested J, Clausen B S, Nielsen L P, Molenbroek A M and Rostrup-Nielsen J R 2002 *J. Catal.* **209** 365
[33] Somers W, Neyts E C, van Duin A C T and Bogaerts A 2012 *J. Phys. Chem. C* (submitted).
[34] Kushner M J 2003 *J. Appl. Phys.* **94** 1436
[35] Mao M and Bogaerts A 2010 *J. Phys. D: Appl. Phys.* **43** 205201
[36] Mao M and Bogaerts A 2010 *J. Phys. D: Appl. Phys.* **43** 315203
[37] Neyts E C, Shibuta Y, van Duin A C T and Bogaerts A 2010 *ACS Nano* **4** 6665
[38] Neyts E C, van Duin A C T and Bogaerts A 2011 *J. Am. Chem. Soc.* **133** 17225
[39] Neyts E C, van Duin A C T and Bogaerts A 2012 *J. Am. Chem. Soc.* **134**, 1256